Journal Name

ARTICLE TYPE

Cite this: DOI: 00.0000/xxxxxxxxxx

Hidden role of Bi incorporation in nonradiative recombination in methylammonium lead iodide

Xie Zhang,*[a] Jimmy-Xuan Shen,[b,c] Mark E. Turiansky,[b] and Chris G. Van de Walle*[a]

Received Date
Accepted Date

DOI: 00.0000/xxxxxxxxxx

Bismuth incorporation has been shown to significantly decrease the performance of perovskite solar cells, which has led to the common belief that Bi_{Pb} is a strong nonradiative recombination center in hybrid perovskites. Using rigorous first-principles calculations, we demonstrate that Bi_{Pb} is *not* an efficient recombination center. However, Bi acts as a donor, and pushes the Fermi level closer to the conduction band; this shift promotes the formation of iodine interstitials, which are the actual nonradiative recombination centers. These insights explain why Bi incorporation is detrimental for the photovoltaic performance. More generally, it draws attention to the detrimental role unintentionally incorporated impurities can play, not by acting as nonradiative recombination centers themselves, but by shifting the Fermi level and thereby promoting the formation of efficiency-killing defects.

Rapidly rising over the past ten years, the power conversion efficiency of perovskite solar cells has reached 25.2%[1]. This efficiency is already close to that of single-crystal silicon cells (26.1%)[1], though instability and toxicity remain as two challenges for perovskite solar cells toward large-scale utilization. In order to further enhance and control their performance, minimizing the nonradiative losses[2] and materials degradation[3] induced by defects or impurities is crucial. Extensive efforts[4–12] have therefore been devoted to revealing the microscopic origins of deep-level defects that may act as nonradiative recombination centers.

In addition to intrinsic defects, extrinsic defects may play an important role. Impurities can be introduced by intentional doping or by unintentional incorporation, for instance, when they are present in precursors. Bismuth has been incorporated into hybrid perovskites in both ways[13–18]. Experiments established that Bi incorporates on the Pb site[18] and significantly reduces the carrier lifetime and power conversion efficiency[16,18]. Hence, it has been proposed[18] that Bi substituting on the Pb site (Bi_{Pb}) acts as a detrimental nonradiative recombination center in hybrid perovskites.

Prior first-principles calculations[18,19] have confirmed that Bi_{Pb} has a charge-state transition level in the band gap, suggesting that Bi_{Pb} may cause nonradiative recombination. However, as we have recently shown[11], the existence of transition levels in the band gap does not necessarily cause nonradiative recombination in halide perovskites. Explicit first-principles calculations of capture coefficients are essential to determine nonradiative recombination rates, and such calculations have not yet been performed for Bi_{Pb}. Here we quantitatively show that Bi_{Pb} itself is *not* a nonradiative recombination center in hybrid perovskites, despite the presence of a charge-state transition level in the band gap. Instead, we attribute the experimentally observed detrimental effect of Bi_{Pb} to the fact that Bi_{Pb} acts as an electrically active center with donor character. The incorporation of Bi therefore shifts the Fermi level closer to the conduction band, which promotes the formation of iodine interstitials (I_i). These intrinsic defects are strong nonradiative recombination centers[12] and the actual cause of the loss in efficiency.

Using the Bi impurity in hybrid perovskites as an example, the present study calls attention to the potentially hidden role of unintentionally incorporated impurities in general. Even though the impurities themselves do not necessarily act as strong nonradiative recombination centers, their presence may shift the Fermi level of the material, which promotes the formation of efficiency-killing defects.

To assess the impact of Bi_{Pb} on nonradiative recombination, we first calculate the formation energy of Bi_{Pb} in the prototypical hybrid perovskite $MAPbI_3$ ($MA=CH_3NH_3$). Figure 1 shows the formation energy of Bi_{Pb} in $MAPbI_3$ as a function of the Fermi

[a] *Materials Department, University of California, Santa Barbara, CA 93106-5050, USA.*
[b] *Department of Physics, University of California, Santa Barbara, CA 93106-9530, USA.*
[c] *Present address: Department of Materials Science and Engineering, University of California, Berkeley, CA 94720, USA.*
* *E-mail: xiezhang@ucsb.edu; vandewalle@mrl.ucsb.edu.*

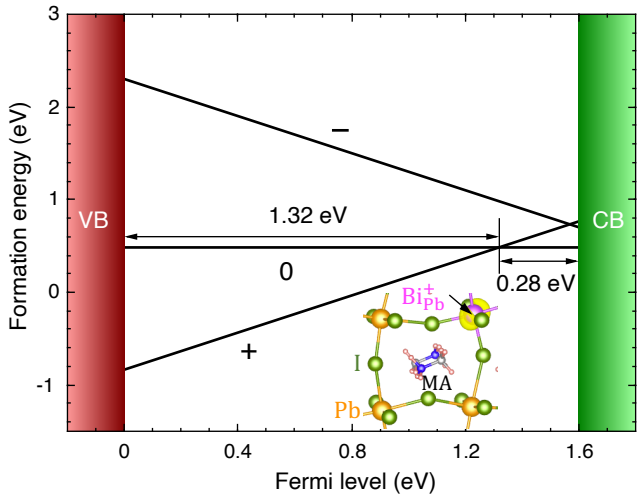

Fig. 1 Formation energy of Bi_{Pb} as a function of the Fermi level in three charge states (+, 0, and −). The $(+/0)$ transition occurs at 0.28 eV below the conduction-band minimum (CBM) or 1.32 eV above the valence-band maximum (VBM). The inset depicts the local atomic structure of Bi^+_{Pb} and the corresponding charge density distribution (yellow isosurface).

level in three relevant charge states (+, 0, and −). Bi_{Pb} favors the + and 0 charge states with a $(+/0)$ transition level at 0.28 eV below the conduction-band minimum (CBM). The formation energy of the − charge state is higher than the energy of the + and 0 states across the entire band gap. Based on the presence of a charge-state transition level in the band gap, Bi_{Pb} was suggested to be a nonradiative recombination center[18]. However, the occurrence of charge-state transition levels in the band gap does not guarantee efficient nonradiative recombination[11,12]; an explicit computation of the capture coefficients is essential.

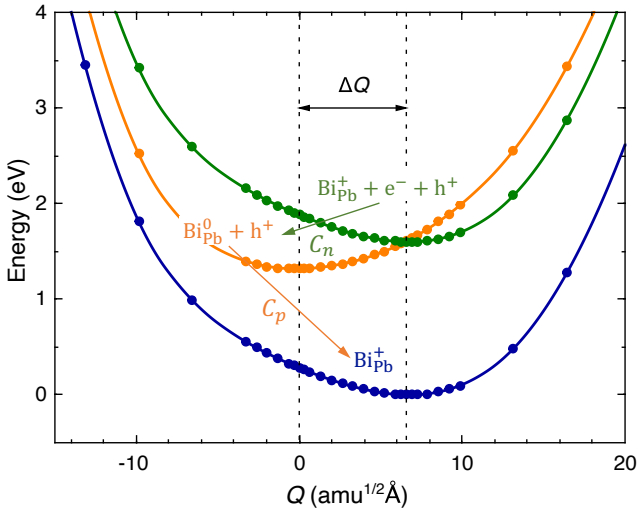

Fig. 2 Configuration coordinate diagram for the $Bi^+_{Pb} \rightleftharpoons Bi^0_{Pb}$ transition accompanied by an electron (C_n) and a hole (C_p) capture processes.

In order to quantitatively determine the capture coefficients, we calculate the configuration coordinate digram for the $Bi^+_{Pb} \rightleftharpoons Bi^0_{Pb}$ transition as shown in Figure 2. This diagram maps the potential energy surfaces of Bi^+_{Pb} and Bi^0_{Pb} as a function of a generalized coordinate (Q). The Q of each configuration is defined by its difference from a reference configuration, i.e., $Q = \sqrt{\sum_\alpha m_\alpha (\mathbf{R}_\alpha - \mathbf{R}_{\mathrm{ref};\alpha})^2}$, where m_α is the mass of atom α and $\mathbf{R}_\alpha$ the Cartesian coordinate of atom α[20]. In Figure 2, $Q = 0$ refers to the equilibrium configuration of Bi^0_{Pb} (the reference configuration) and $Q = \Delta Q$ corresponds to that of Bi^+_{Pb}. The configuration coordinate diagram allows us to inspect the charge-state transitions and the accompanying electron/hole capture processes.

Starting from Bi^+_{Pb} with an electron (e^-) at the CBM and a hole (h^+) at the VBM (the green curve in Figure 2), Bi^+_{Pb} can capture the electron and transition to Bi^0_{Pb} (the orange curve in Figure 2). Subsequently, Bi^0_{Pb} captures the hole and transforms back to Bi^+_{Pb} (the blue curve in Figure 2). Semiclassically, the capture rate is characterized by the energy barrier for the charge-state transition, i.e., the energy required to cross the intersection of the potential energy surfaces between the initial and final charge states in the configuration coordinate diagram. In the present case, the electron capture barrier is almost zero and the hole capture barrier is extremely large (>2.7 eV), since the orange and blue curves do not even intersect within the range of Q displayed in Figure 2. This implies fast electron capture and slow hole capture; this is consistent with the position of the charge-state transition level in the band gap (Figure 1), since the capture coefficient is expected to decrease with increasing transition energy[21].

An important feature here is that the potential energy surfaces of Bi_{Pb} are highly anharmonic. The pronounced anharmonicity significantly decreases the potential energy of Bi^+_{Pb} in the vicinity of the equilibrium configuration of Bi^0_{Pb}, which leads to a much larger energy barrier for the $Bi^0_{Pb} \rightarrow Bi^+_{Pb}$ transition than in a harmonic case. Hole capture is already expected to be slow since the $(+/0)$ transition level is 1.32 eV away from the VBM (Figure 1). The strong anharmonicity makes hole capture even slower.

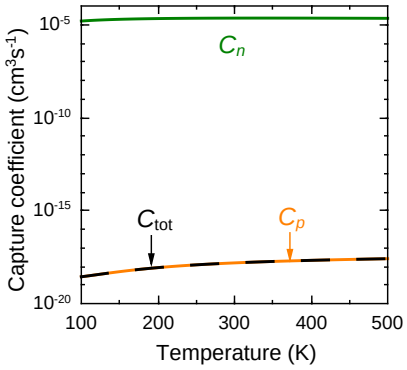

Fig. 3 Nonradiative electron (green), hole (orange), and total (black) capture coefficients of Bi_{Pb} as a function of temperature.

In Figure 3 we present the calculated nonradiative capture coefficients of Bi_{Pb}. Consistent with our analysis of the capture barriers, the electron capture coefficient (C_n) is very high, on the order of 10^{-5} cm^{3}s^{-1}, while the hole capture coefficient (C_p) is much lower, on the order of 10^{-18} cm^{3}s^{-1} at room temperature. The total capture coefficient is determined by $C_{tot} = C_n C_p/(C_n + C_p)$, and is limited by hole capture in the present case. Therefore, the total

capture coefficient is only $\sim 10^{-18}$ cm^{3}s^{-1} at room temperature.

The nonradiative recombination coefficient (A) is related to the total capture coefficient through $A = N_{\rm def} C_{\rm tot}$, where $N_{\rm def}$ is the defect concentration. Even if we assume an unrealistically high concentration of Bi_{Pb}, e.g., 10^{20} cm^{-3}, the resulting A coefficient is only about 10^2 s^{-1}, which is five orders of magnitude lower than reported experimental nonradiative recombination coefficients of intrinsic hybrid perovskites ($\sim 10^7$ s^{-1} [22–26]). This means that Bi_{Pb} is not an efficient nonradiative recombination center.

Experimentally, it has been observed that the incorporation of Bi significantly decreases the carrier lifetime and power conversion efficiency of perovskite solar cells [16,18]. Based on our accurate calculations, this observation cannot be attributed to the nonradiative recombination caused by Bi_{Pb}, raising the question: why does Bi_{Pb} affect the nonradiative recombination in hybrid perovskites, even though it is not an efficient recombination center?

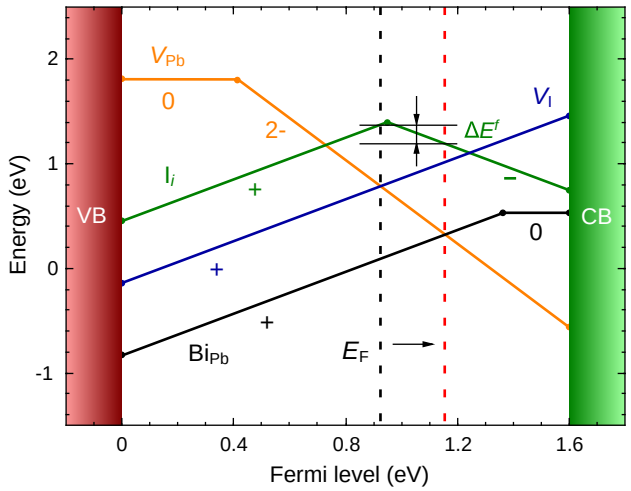

Fig. 4 Impact of Bi_{Pb} on the Fermi-level position in $MAPbI_3$. The black (red) dashed line shows the location at which the Fermi level is pinned without (with) the incorporation of Bi. ΔE^f denotes the change in the formation energy of I_i due to the shift of the Fermi level.

To answer this question, we plot the formation energy of Bi_{Pb} together with those of the three dominant intrinsic defects in $MAPbI_3$ (I_i, V_{Pb}, and V_I) in Figure 4. In this diagram, we can determine the position of the Fermi level in the material based on charge neutrality between the lowest-energy defects. Without Bi incorporation, the Fermi level is pinned by V_I and V_{Pb}, as depicted by the black dashed line in Figure 4. After introducing Bi into the material, the Fermi level is pinned by Bi_{Pb} and V_{Pb} (the red dashed line in Figure 4), which shifts the Fermi level toward the CBM by 0.23 eV.

While V_{Pb} is the lowest-energy intrinsic defect, it does not cause significant nonradiative recombination in $MAPbI_3$; I_i is a dominant recombination center that is likely responsible for the experimentally measured A coefficient in hybrid perovskites [12]. As shown in Figure 4, the formation energy of I_i is reduced by 0.2 eV due to the incorporation of Bi. The defect concentration is proportional to $e^{-E^f/k_B T}$, where k_B is the Boltzmann constant. T is the growth temperature, which is around 150 °C [9] for hybrid perovskites. Hence, a reduction of the formation energy (ΔE^f) of I_i by 0.2 eV means an enhancement of its concentration by a factor of 242. This implies that the nonradiative recombination coefficient induced by I_i will be increased by more than two orders of magnitude, which will clearly impact the carrier lifetime and power conversion efficiency. We note that the Fermi-level shift also depends on the concentration of Bi. A higher concentration of Bi will shift the Fermi level toward the CBM even further, which results in an even stronger enhancement of the concentration of I_i.

In summary, we have explained the mechanism by which incorporation of Bi in hybrid perovskites causes a drop in efficiency. Our explicit first-principles calculations show that even though Bi_{Pb} has a charge-state transition level in the band gap in $MAPbI_3$, it does *not* act as a nonradiative recombination center. The true cause of the efficiency reduction is a Bi-induced enhancement in the concentration of iodine interstitials, which act as strong nonradiative recombination centers. The enhancement is due to a shift of the Fermi level, resulting from Bi acting as a donor. Our results focus attention on the detrimental role unintentionally incorporated impurities can play, not by acting as nonradiative recombination centers, but by shifting the Fermi level and thereby promoting the formation of efficiency-killing defects—in this case, iodine interstitials. Therefore, to control the incorporation of iodine interstitial defects I-poor synthesis conditions are, in principle, desired. However, we also note that I-poor conditions may promote the formation of iodine vacancies, which may degrade the performance of hybrid perovskites. A careful optimization of the synthesis condition is required to minimize the detrimental impacts of iodine interstitials and vacancies.

Methods

The first-principles calculations in this work are performed using density functional theory with the Heyd-Scuseria-Ernzerhof (HSE) functional [27], including spin-orbit coupling (SOC), as implemented in the Vienna *Ab-initio* Simulation Package (VASP) [28]. Additional computational details can be found in Refs. 11,12. The chemical potential of Bi ($\mu_{\rm Bi}$) is chosen to reflect equilibrium with BiI_3: $\mu_{\rm Bi} + 3\mu_{\rm I} = \Delta H_f(BiI_3) = -1.86$ eV, where $\mu_{\rm I}$ is the chemical potential of iodine and $\Delta H_f(BiI_3)$ the calculated formation enthalpy of BiI_3. For the host chemical potentials, we choose $\mu_{\rm I}$ to correspond to I-medium conditions, which are representative of typical synthesis. The nonradiative capture coefficients are calculated using the multiphonon emission methodology [20] with an extension to anharmonic potential energy surfaces [11,12].

Conflicts of interest

There are no conflicts to declare.

Acknowledgements

This work was supported by the U.S. Department of Energy (DOE), Office of Science, Basic Energy Sciences (BES) under Award No. DE-SC0010689. Computational resources were provided by the National Energy Research Scientific Computing Center, a DOE Office of Science User Facility supported by the Office of Science of the U.S. Department of Energy under Contract No. DE-AC02-05CH11231.

Notes and references

1 *Best Research-Cell Efficiency Chart*, https://www.nrel.gov/pv/assets/pdfs/best-research-cell-efficiencies.20200203.pdf, Accessed: 2020-02-03.

2 X. Zhang, J.-X. Shen and C. G. Van de Walle, *Adv. Energy Mater.*, 2020, **10**, 1902830.

3 N. Aristidou, C. Eames, I. Sanchez-Molina, X. Bu, J. Kosco, M. S. Islam and S. A. Haque, *Nat Commun*, 2017, **8**, 15218.

4 W.-J. Yin, T. Shi and Y. Yan, *Appl. Phys. Lett.*, 2014, **104**, 063903.

5 A. Buin, P. Pietsch, J. Xu, O. Voznyy, A. H. Ip, R. Comin and E. H. Sargent, *Nano Lett.*, 2014, **14**, 6281–6286.

6 M.-H. Du, *J. Phys. Chem. Lett.*, 2015, **6**, 1461–1466.

7 A. Baumann, S. Väth, P. Rieder, M. C. Heiber, K. Tvingstedt and V. Dyakonov, *J. Phys. Chem. Lett.*, 2015, **6**, 2350–2354.

8 S. Heo, G. Seo, Y. Lee, D. Lee, M. Seol, J. Lee, J.-B. Park, K. Kim, D.-J. Yun, Y. S. Kim, J. K. Shin, T. K. Ahn and M. K. Nazeeruddin, *Energy Environ. Sci.*, 2017, **10**, 1128–1133.

9 W. S. Yang, B.-W. Park, E. H. Jung, N. J. Jeon, Y. C. Kim, D. U. Lee, S. S. Shin, J. Seo, E. K. Kim, J. H. Noh and S. I. Seok, *Science*, 2017, **356**, 1376–1379.

10 D. Meggiolaro, S. G. Motti, E. Mosconi, A. J. Barker, J. Ball, C. Andrea Riccardo Perini, F. Deschler, A. Petrozza and F. De Angelis, *Energy Environ. Sci.*, 2018, **11**, 702–713.

11 X. Zhang, M. E. Turiansky and C. G. Van de Walle, *J. Phys. Chem. C*, 2020, **124**, 6022–6027.

12 X. Zhang, M. E. Turiansky, J.-X. Shen and C. G. Van de Walle, *Phys. Rev. B*, 2020, **101**, 140101.

13 A. L. Abdelhady, M. I. Saidaminov, B. Murali, V. Adinolfi, O. Voznyy, K. Katsiev, E. Alarousu, R. Comin, I. Dursun, L. Sinatra, E. H. Sargent, O. F. Mohammed and O. M. Bakr, *J. Phys. Chem. Lett.*, 2016, **7**, 295–301.

14 Y. Yamada, M. Hoyano, R. Akashi, K. Oto and Y. Kanemitsu, *J. Phys. Chem. Lett.*, 2017, **8**, 5798–5803.

15 Y. Hu, F. Bai, X. Liu, Q. Ji, X. Miao, T. Qiu and S. Zhang, *ACS Energy Lett.*, 2017, **2**, 2219–2227.

16 P. K. Nayak, M. Sendner, B. Wenger, Z. Wang, K. Sharma, A. J. Ramadan, R. Lovrinčić, A. Pucci, P. K. Madhu and H. J. Snaith, *J. Am. Chem. Soc.*, 2018, **140**, 574–577.

17 J. Yin, G. H. Ahmed, O. M. Bakr, J.-L. BrÃľdas and O. F. Mohammed, *ACS Energy Lett.*, 2019, **4**, 789–795.

18 M. Yavari, F. Ebadi, S. Meloni, Z. S. Wang, T. C.-J. Yang, S. Sun, H. Schwartz, Z. Wang, B. Niesen, J. Durantini, P. Rieder, K. Tvingstedt, T. Buonassisi, W. C. H. Choy, A. Filippetti, T. Dittrich, S. Olthof, J.-P. Correa-Baena and W. Tress, *J. Mater. Chem. A*, 2019, **7**, 23838–23853.

19 J.-L. Li, J. Yang, T. Wu and S.-H. Wei, *J. Mater. Chem. C*, 2019, **7**, 4230–4234.

20 A. Alkauskas, Q. Yan and C. G. Van de Walle, *Phys. Rev. B*, 2014, **90**, 075202.

21 C. H. Henry and D. V. Lang, *Phys. Rev. B*, 1977, **15**, 989–1016.

22 Y. Yamada, T. Nakamura, M. Endo, A. Wakamiya and Y. Kanemitsu, *J. Am. Chem. Soc.*, 2014, **136**, 11610–11613.

23 R. L. Milot, G. E. Eperon, H. J. Snaith, M. B. Johnston and L. M. Herz, *Adv. Funct. Mater.*, 2015, **25**, 6218–6227.

24 D. Bi, W. Tress, M. I. Dar, P. Gao, J. Luo, C. Renevier, K. Schenk, A. Abate, F. Giordano, J.-P. Correa Baena, J.-D. Decoppet, S. M. Zakeeruddin, M. K. Nazeeruddin, M. Grätzel and A. Hagfeldt, *Sci. Adv.*, 2016, **2**, e1501170–e1501170.

25 J. M. Richter, M. Abdi-Jalebi, A. Sadhanala, M. Tabachnyk, J. P. Rivett, L. M. Pazos-Outón, K. C. Gödel, M. Price, F. Deschler and R. H. Friend, *Nat. Commun.*, 2016, **7**, 13941.

26 H. Zhu, M. T. Trinh, J. Wang, Y. Fu, P. P. Joshi, K. Miyata, S. Jin and X. Y. Zhu, *Adv. Mater.*, 2017, **29**, 1603072.

27 J. Heyd, G. E. Scuseria and M. Ernzerhof, *J. Chem. Phys.*, 2003, **118**, 8207–8215.

28 G. Kresse and J. Furthmüller, *Phys. Rev. B*, 1996, **54**, 11169–11186.